American Mineralogist, Volume 82, pages 534–545, 1997

Minor and trace element partitioning between pyroxene and melt in rapidly cooled chondrules

RHIAN H. JONES[1] **AND GRAHAM D. LAYNE**[1,2]

[1]Institute of Meteoritics, Department of Earth and Planetary Sciences, University of New Mexico, Albuquerque, New Mexico 87131, U.S.A.
[2]Department of Geology and Geophysics, Woods Hole Oceanographic Institution, Woods Hole, Massachusetts 02543-1541, U.S.A.

ABSTRACT

We present minor and trace element (REE, Sr, Y, and Zr) data for pyroxenes and mesostases in four porphyritic chondrules from the Semarkona ordinary chondrite. Apparent partition coefficients for clinoenstatite, orthoenstatite, pigeonite, and augite are compared with experimental and petrologic data from the literature, and the effects on apparent partition coefficients of the rapid cooling rates at which chondrules crystallized are evaluated. For most elements, the effects of cooling at rates of hundreds of degrees per hour cannot be distinguished from variations in equilibrium data resulting from differences in temperature or composition. However, for LREE apparent partition coefficients are significantly higher than comparable equilibrium data, and the ratio of HREE/LREE partition coefficients is lower, particularly for Ca-poor pyroxene. We attribute this flattening of REE patterns to the effect of rapid cooling. Apparent partition coefficients of all REE and Y in augite are higher than equilibrium data, particularly in one chondrule with a high Al_2O_3 content. We suggest that this may be attributed to an increase in the uptake of trivalent trace element cations in the pyroxene crystal structure as a result of charge-balanced substitutions with Al^{3+} cations.

INTRODUCTION

Chondrules are millimeter-sized silicate spherules that are ubiquitous in chondritic meteorites. They are thought to have formed in the solar nebula at 4.6 Ga when free-floating dust balls entrained in the nebular gas were flash heated and melted, then cooled rapidly (Grossman 1988). The chondrule mineral assemblage is dominated by olivine and pyroxene, and textures range from fine-grained, cryptocrystalline to coarse-grained, porphyritic varieties. The extent of mass loss from chondrules by evaporation at temperatures close to peak temperatures has been a subject of considerable recent discussion (Alexander 1996; Sears et al. 1996). However, many porphyritic chondrules may be considered to have behaved essentially as closed igneous systems during most of the crystallization interval (Jones 1996). This provides an opportunity to examine partitioning behavior during fractional crystallization, with few ambiguities about the extent of the closed system. Although moderately volatile elements such as Na may have undergone subsolidus redistribution, either in the nebula or on the parent body (Matsunami et al. 1993; Grossman 1996), most minor and trace elements of geologic interest would not have been affected by such processes. In this paper, we present minor and trace element analyses of pyroxene and mesostasis in four porphyritic, pyroxene- and olivine-bearing chondrules from the Semarkona LL ordinary chondrite. These data allow us to examine the effect of rapid cooling on minor and trace element partitioning behavior, as well as the effect of melt composition that varies between individual chondrules. Semarkona is one of the least equilibrated ordinary chondrites (petrologic type 3.0), in which chondrules are essentially unaffected by any secondary processing such as thermal metamorphism or aqueous alteration. Few other trace element data are available for individual chondrule phases: the most comprehensive study is that of Alexander (1994), who presented trace element data for olivine, pyroxene, and glass from chondrules in three ordinary chondrites, Semarkona (LL3.0), Bishunpur (LL3.2), and Chainpur (LL3.4). Our data may be compared with data from systems of comparable composition that are available from petrological and experimental studies.

ANALYTICAL TECHNIQUES

The chondrules studied were selected from a polished thin section of Semarkona, UNM 620. Electron microprobe analyses were carried out for major and minor elements, and ion microprobe analyses were performed for trace elements including rare earth elements (REE), Sr, Y, and Zr.

Major and minor element analyses of minerals and mesostasis, and backscattered electron (BSE) imaging, were carried out on a JEOL 733 Superprobe, operating at 15 kV and 20 nA. Silicate minerals such as olivine, pyroxene, and feldspar were used as standards, and analyses of

0003–004X/97/0506–0534$05.00

secondary standards were performed to verify the analysis procedure. Counting times up to 40 s were used for minor elements. Most analyses were performed by WD spectrometry, using ZAF correction procedures on an Oxford/Link LEMAS EXL operating system. Some data were acquired by combined ED/WD analysis (ED for major elements) on the same system, and no differences were observed between the two types of analyses. Data acquired before December 1992, were obtained using WD analysis and reduced using the Bence-Albee correction procedure, using a Tracor-Northern TN 2000 operating system. The two operating systems gave results that were identical within analytical errors on the same chondrule phases. A beam diameter of 1 μm was used for silicate minerals, and 10 μm for mesostasis. Mesostasis analyses are average compositions of glass plus quench crystals and reflect the compositions of the final liquids in the chondrules at the point when phenocryst crystallization ceased. Typical detection limits (wt%) were as follows: TiO_2, 0.02; Al_2O_3 and Cr_2O_3, 0.03; MnO and CaO, 0.04; and Na_2O, 0.05.

Trace element analyses were performed by Secondary Ion Mass Spectrometry (SIMS) using the Cameca IMS 4f instrument operated by the University of New Mexico/Sandia National Laboratories Ion Microprobe Facility. Grain areas free of cracks and inclusions were preselected using SEM. Secondary ion imaging of major elements was used to position the ion beam for each analysis to avoid contamination from adjacent phases. Pyroxenes and mesostases were analyzed for Sr, Y, Zr, and eight REE (La, Ce, Nd, Sm, Eu, Dy, Er, and Yb). Analyses were made by bombardment of the sample with primary O^- ions accelerated through a nominal potential of 10kV. Primary ion currents between 5 and 40 nA were selected, depending on the maximum spot size practical for each individual analysis. Typical pit diameters for completed analyses were 50 μm for Ca-poor pyroxene, 30 μm for pigeonite, 1 μm for augite, and 10–50 μm for mesostasis.

Each analysis involved repeated cycles of peak counting on $^{30}Si^+$, $^{88}Sr^+$, $^{89}Y^+$, $^{90}Zr^+$, $^{139}La^+$, $^{140}Ce^+$, $^{146}Nd^+$, $^{147}Sm^+$, $^{151}Eu^+$, $^{153}Eu^+$, $^{163}Dy^+$, $^{167}Er^+$, and $^{174}Yb^+$, as well as counting on a background position to monitor detection noise. Individual cycles were monitored to detect any obvious contamination from the primary beam penetrating an adjacent phase during the progress of the analysis. Sputtered secondary ions were energy filtered using a sample offset voltage of −75 V and an energy window of ±25 V effectively to eliminate isobaric interferences.

Ba concentrations were not measured directly because the installed software on the IMS 4f limits the number of analytical peaks to 14. For pyroxenes, where Ba/Eu is commonly $\ll 0.1$, a correction for Ba on Eu is not necessary. However, for mesostasis, where Ba/Eu is expected to be >10, an empirical correction for the effect of $^{135}BaO^+$ and $^{137}BaO^+$ on the $^{151}Eu^+$ and $^{153}Eu^+$ peaks was necessary. A matrix solution correction was applied using accepted natural abundance ratios for Ba and Eu ($^{135}Ba/^{137}Ba$ of 0.5822, $^{151}Eu/^{153}Eu$ of 0.9146). This method has an advantage in comparison with direct correction using measured Ba^+ peaks, because it does not depend directly on the BaO^+/Ba^+ ratio, which is quite sensitive to variations in chemical matrix and energy offset.

For mesostasis, typical precisions were better than 1% for Sr, 2% for Y and Zr, 2–5% for LREE and Eu, and 5–10% for HREE. For Ca-rich pyroxene typical precisions were better than 2–5% for Sr, 3–7% for Y and Zr, 8% for Ce, and 10–20% for the other REE. For Ca-poor pyroxene precisions for Sr and Y were typically better than 10–15%. Precisions for the other elements analyzed were typically worse than 10–20%, with concentrations often approaching or falling below the analytical detection limit.

Detection limits were assessed in the following manner. Instrumental noise, which was measured at a background position during each cycle of each analysis, was typically 1–2 counts per min. The estimated detection limit was calculated as the apparent concentration of each element that would be derived by processing a signal equivalent to the mean background plus two times the standard deviation of the background, as calculated from the background measurements of all analyses in a session. Typical detection limits for 12 cycles of analysis (1 h) were below 1 ppb for Sr, Y, Zr, La, and Ce; 1–2 ppb for Eu and Yb; 2–4 ppb for Nd, Dy, and Er; and 3–5 ppb for Sm.

Absolute concentrations of each element were calculated using empirical relationships between measured peak/$^{30}Si^+$ ratios (normalized to known SiO_2 content measured with the electron microprobe) and element concentrations, as derived from measurements of documented pyroxene and basalt standards. Kilbourne Hole augite (Irving and Frey 1984) was used as a standard for all pyroxenes. Although Gd was not analyzed, for plotting purposes, it was estimated for some analyses by log-linear interpolation between Nd and Dy (mesostasis) or Sm and Dy (pyroxene). No correction for the interference of $^{158}GdO^+$ on $^{174}Yb^+$ was made. For flat REE patterns, e.g., mesostasis, the contribution of this interference to $^{174}Yb^+$ is less than 7%, and for the LREE depleted patterns of Ca-poor pyroxenes, the contribution is less than 2–3%.

Results

Chondrule textures

Detailed descriptions of the chondrules included in this study have been presented previously (Jones 1994, 1996), and only a brief summary of their petrology is given here. All the chondrules are considered to have crystallized from essentially entirely molten droplets. Recognizable relict grains, typically olivine, that survived chondrule formation are rare. Two relict olivines occur in chondrule 111 (Jones 1996). Relict grains appear to have undergone a limited degree of resorption into the chondrule melts at high temperatures but are overgrown with olivine that crystallized during the cooling interval. Thus they were isolated from the melt during crystallization and did not cause further changes in melt compositions. Olivine com-

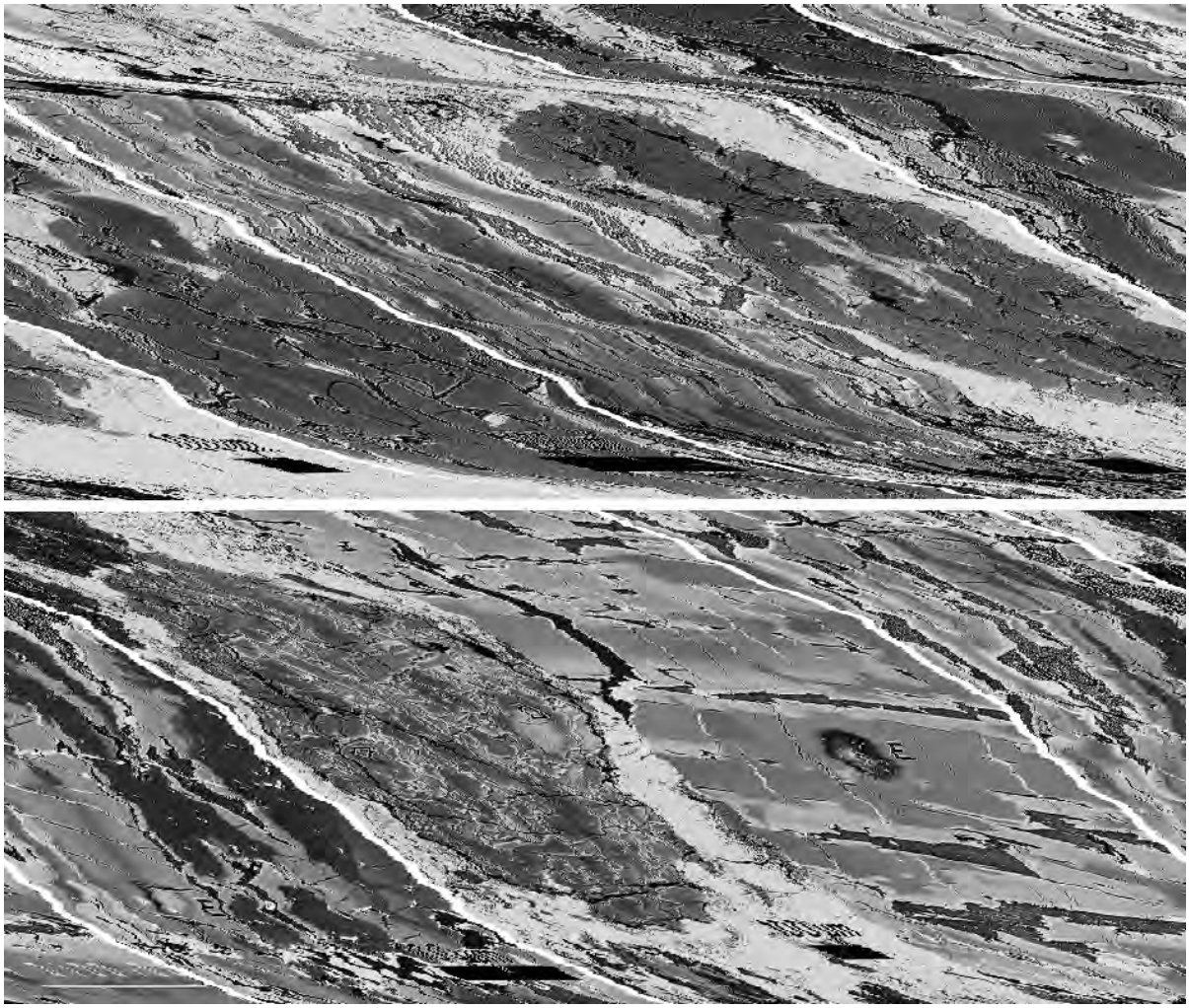

FIGURE 1. BSE images showing the textures of the chondrules analyzed. All the chondrules contain pyroxene phenocrysts in a glassy mesostasis containing quench crystallites. Circles indicate SIMS analysis points and approximate sizes of the ion beam pits: A = augite, P = pigeonite, E = orthoenstatite, C = clinoenstatite, and M = mesostasis. Olivine phenocrysts (O) are also present in three of the chondrules. (**a**) Chondrule 20, consisting of olivine and clinoenstatite phenocrysts and interstitial glassy mesostasis. Augite (white) commonly occurs as overgrowths on clinoenstatite. (**b**) Chondrule 20, showing the positions of several SIMS analyses. Euhedral clinoenstatite phenocrysts show lamellar zoning (Jones 1994). (**c**) Chondrule 70. Coarse bars of pyroxene consist of clinoenstatite cores overgrown successively with orthoenstatite, pigeonite, and narrow augite rims (Jones 1996). (**d**) Chondrule 70, showing a SIMS analysis pit on an orthoenstatite grain. In **d** and **e**, the white material in cracks is the remnant of the gold coatings applied for SIMS analysis. (**e**) Chondrule 71, also showing a SIMS analysis pit on an orthoenstatite grain. Two SIMS analyses were run on the mesostasis, but these used substantially lower primary beam currents and shorter analysis times, and the resulting pits are not readily visible. Texture is similar to chondrule 70 (**b** and **c**). (**f**) Chondrule 111. Pyroxene and olivine phenocrysts in a glassy mesostasis. Two olivine grains have relict olivine cores (arrowed). All scales are 100 μm.

positions and zoning behavior in these chondrules are described by Jones (1994, 1996).

Chondrule 20 (Fig. 1a and b) is an FeO-poor, porphyritic, pyroxene+olivine chondrule (mg no. > 90 in silicate minerals). It contains large (up to 200 μm) phenocrysts of clinoenstatite that have augite overgrowths on their rims (Jones 1994). Smaller olivine phenocrysts are also present, and some olivine is poikilitically enclosed in pyroxene phenocrysts. Mesostasis is glassy and contains microcrystalline quench crystals. Minor iron nickel metal and sulfide blebs are present throughout the chondrule.

Chondrules 70, 71, and 111 are FeO-rich (mg no. < 90 in silicate minerals). Chondrules 70 and 71 (Figs. 1c–e) have ''coarse barred'' textures, with sets of subparallel pyroxene bars dominating the texture (Jones 1996). Pyroxene bars are up to 1 mm long and 100 μm wide. In chondrule 71, olivine is present both as euhedral phenocrysts and as bars intergrown with the pyroxene. Chon-

drule 70 does not contain olivine. In both chondrules, pyroxene phenocrysts show complex zoning and consist of clinoenstatite cores overgrown successively with orthorhombic enstatite, pigeonite, and narrow augite rims. Mesostases are glassy with abundant quench microcrystallites, and minor iron nickel metal and sulfides are present.

Chondrule 111 (Fig. 1f) contains pyroxene and olivine in approximately equal proportions (Jones 1996). Olivine phenocrysts have hopper morphologies, and pyroxene is present as euhedral grains and elongate laths. Pyroxene phenocrysts consist of clinoenstatite cores overgrown with pigeonite, and narrow augite rims. Mesostasis is glassy with abundant quench microcrystallites, and minor iron nickel metal and sulfides are present.

Pyroxene and mesostasis compositions

Compositions of pyroxenes and mesostases are presented in Tables 1 and 2. Data in Table 1 are reported as mean compositions of individual phases. For major and minor element contents, determined by electron microprobe analysis, these mean values include 4–10 random points obtained for each phase in individual chondrules. Trace element analyses are either single points, or means of up to three analyses, and are given as abundances relative to abundances in CI chondrites (Anders and Grevesse 1989). Table 2 gives representative, individual electron microprobe analyses for some of the pyroxenes at or near the positions of the SIMS analyses. In general, these compositions lie within one standard deviation of the means given in Table 1.

Pyroxenes in the chondrules studied show variable zoning behavior, which has been discussed extensively previously (Jones 1994, 1996). The nature and extent of the zoning present clearly has an impact on the interpretation of the trace element analyses, which use broad SIMS analysis spots. Standard deviations on mean major element pyroxene compositions given in Table 1 reflect the extent of zoning observed in each phase. In general, Ca-poor pyroxenes show very limited zoning from cores to edges of grains. For example, individual analyses from the core and edge of a grain close to a SIMS analysis pit in chondrule 20 are given in Table 2 and show that core-to-edge zoning is essentially absent. However, clinoenstatite in chondrule 20 shows lamellar zoning in BSE images (Fig. 1b), on a scale of <20 μm, and parallel to (001), which reflects limited compositional zoning for FeO and minor elements and is the main source of the variation about the mean given in Table 1. SIMS analyses average the composition of Fe-poor and Fe-rich lamellae in these grains. In contrast, augites show relatively strong zoning from their inner contact with Ca-poor pyroxenes to their outer edges in contact with mesostasis. Concentrations of CaO, Al_2O_3, TiO_2, and Na_2O may increase by factors of two to four from inner to outer edge, over a distance of 10–20 μm. SIMS analyses of augites are thus necessarily averages over this compositional range. Hence, the individual analysis points given in Table 2 cannot be compared directly with the SIMS data in most cases, because the SIMS data cover a wider range of compositions than electron microprobe analyses. The mean electron microprobe analyses given in Table 1 are more representative of the compositions analyzed by SIMS, and we refer to these data throughout the remainder of the paper. We recognize that for purposes of discussion of apparent partition coefficients, the data for augites are likely to be minimum values. Because values of D^* for many of the trace elements are similar to those of minor elements such as Al, Ti, and Na in augites (Table 3; see below), similar degrees of zoning may be expected and this could result in errors in D^* by up to a factor of two. However, for Ca-poor pyroxenes the measured compositions are likely to be very similar to true edge compositions, and errors in apparent partition coefficients arising from zoning are not likely to be significant.

Minor element contents (TiO_2, Al_2O_3, Cr_2O_3, MnO, and Na_2O) of pyroxenes in each chondrule increase with Wo content (Table 1). Some minor element contents vary significantly between chondrules, for example the average Al_2O_3 content of augite varies from 1 wt% in chondrules 70 and 111 to 7 wt% in chondrule 20. High average Al_2O_3 contents in all pyroxenes in chondrules 20 and 71 are consistent with the high average Al_2O_3 contents of mesostases in these chondrules (19 and 18 wt%, respectively).

Various REE abundance diagrams for individual chondrules are illustrated in Figure 2, which shows individual analyses as well as the mean compositions given in Table 1. For mesostasis in chondrule 70, two analyses with analysis pits 10 and 50 μm wide gave indistinguishable results, indicating that the analytical volumes were successfully averaging glass plus quench crystals and may be considered to represent final liquid compositions. For mesostasis in chondrule 20, two analyses with similar pit diameters gave slightly different results, which is probably attributable to different concentrations of quench crystals in each spot. The REE contents of pyroxenes increase with Wo content: for Ca-poor pyroxenes (clinoenstatite and orthopyroxene), REE abundances lie in the range 0.01 to 0.1 relative to CI, and for augite, REE abundances are approximately 1–10 $\times$ CI abundances. REE abundances in augite (the smallest grains measured) do not appear to be compromised by the possibility of ion beam overlap with mesostasis, because different analyses give consistent REE abundances (chondrule 20). For Ca-poor pyroxene, REE are often close to or below detection limits, and in the pigeonite measured (chondrule 70), Eu is below detection limits, implying a negative Eu anomaly. Augite also shows negative Eu anomalies in chondrules 20 and 111. REE abundances in mesostases are enriched, at approximately 10 $\times$ CI abundances, and show relatively flat patterns, sometimes with very small positive Eu anomalies that are complementary to the pyroxene.

TABLE 1. Mean compositions of chondrule pyroxenes and mesostases

	Chondrule 20			Chondrule 70				
	Aug	Cen	Meso	Aug	Pig	Opx	Cen	Meso
SiO_2	49.9(0.8)	58.7(0.5)	57.0(0.5)	51.7(0.2)	53.4(0.3)	55.8(0.5)	56.9(0.3)	64.2(2.3)
TiO_2	0.88(0.15)	0.07(0.01)	0.47(0.15)	0.19(0.10)	0.09(0.03)	0.03(0.01)	0.02(0.01)	0.44(0.08)
Al_2O_3	7.1(1.4)	0.45(0.14)	19.4(0.1)	1.0(0.5)	0.66(0.20)	0.17(0.04)	0.08(0.05)	9.6(1.0)
Cr_2O_3	2.7(0.3)	0.68(0.14)	0.22(0.06)	1.8(0.5)	1.0(0.1)	0.73(0.09)	0.54(0.04)	0.05(0.04)
FeO	1.9(0.2)	1.8(0.17)	2.3(0.5)	19.1(1.3)	19.1(0.6)	13.6(0.9)	11.4(0.7)	14.5(2.0)
MnO	0.99(0.17)	0.30(0.12)	0.88(0.07)	1.12(0.11)	0.92(0.07)	0.57(0.07)	0.40(0.05)	0.58(0.15)
MgO	17.0(1.1)	37.9(0.4)	3.0(0.2)	14.0(1.5)	20.3(0.9)	28.4(0.7)	30.3(0.6)	0.37(0.51)
CaO	19.4(0.8)	0.26(0.09)	10.3(0.4)	11.4(0.9)	4.1(0.6)	0.29(0.08)	0.11(0.04)	4.0(1.3)
Na_2O	0.16(0.03)		4.5(0.2)	0.35(0.05)	0.08(0.04)			4.8(0.8)
K_2O			0.23(0.02)					0.71(0.11)
Sr	3.90(0.82)	0.026(0.003)	12.0(1.1)	1.71(0.15)	0.15(0.01)	0.008(0.005)	0.039(0.004)	7.65(0.10)
Y	10.4(0.96)	0.052(0.013)	10.3(2.1)	2.43(0.46)	0.49(0.04)	0.050(0.027)	0.025(0.005)	6.58(0.32)
Zr	9.47(1.33)	0.041(0.014)	11.4(1.4)	1.33(0.15)	0.091(0.015)	0.016(0.010)	0.022(0.006)	7.13(0.25)
La	4.35(0.84)	0.009(0.004)	13.0(1.6)	0.66(0.16)	0.050(0.011)	0.010(0.004)	0.016(0.008)	7.76(0.29)
Ce	5.61(1.12)	0.020(0.005)	13.8(2.3)	1.20(0.25)	0.073(0.011)	0.011(0.004)	0.011(0.004)	8.07(0.12)
Nd	7.11(1.38)	0.015(0.008)	13.0(1.6)	1.62(0.53)	0.078(0.029)	0.024(0.002)		8.53(0.45)
Sm	9.78(1.40)		16.3(7.1)	1.96(0.71)				7.76(0.38)
Eu	5.76(1.53)		11.7(2.6)	1.90(0.68)				6.87(0.90)
Gd*	10.1		11.6	2.11				7.21
Dy	10.4(1.2)		11.2(2.6)	2.26(0.57)	0.219(0.066)	0.072(0.007)	0.028(0.013)	6.66(0.48)
Er	10.1(0.9)	0.043(0.019)	9.8(3.1)	2.46(0.96)	0.467(0.098)	0.088(0.037)		7.22(0.31)
Yb	8.21(0.8)	0.125(0.015)	10.4(2.6)	2.27(0.32)	0.484(0.087)	0.097(0.034)	0.092(0.040)	7.50(0.15)
En	53.0	96.9		42.5	59.8	78.4	82.5	
Fs	3.2	2.6		32.6	31.6	21.1	17.3	
Wo	43.8	0.5		24.9	8.7	0.6	0.2	
n	8, 3	7, 2	4, 2	5, 1	5, 1	10, 3	6, 1	10, 2

Notes: Aug = augite, Pig = pigeonite, Cen = clinoenstatite, Opx = orthopyroxene, Meso = mesostasis. Oxide contents in wt% (electron microprobe analyses), from Jones (1994) for chondrule 20 and Jones (1996) for chondrules 70, 71, and 111. Trace element contents (ion microprobe analyses) are given as abundances relative to CI (Anders and Grevesse 1989). n = number of points for major and trace element analyses respectively. Numbers in parentheses are 1σ standard deviations for averages of 2 or more data points. For single analyses by SIMS, the numbers in parentheses represent the analytical precision as derived from the standard error of the mean of individual cycles of peak counting.

* Gd contents are estimated. Blank spaces indicate concentration below detection limit.

Apparent partition coefficients

Apparent partition coefficients (D*) for pyroxene-melt are given in Table 3. These values are calculated as the ratio (mean mineral composition)/(mean mesostasis composition), using weight ratios. During the chondrule crystallization interval, the composition of liquid changes from that of essentially the bulk chondrule composition to that of the final liquid, represented by the present mesostasis. Late-stage augite clearly crystallized from a melt of composition close to that of the mesostasis. However, Ca-poor pyroxene began to crystallize at the beginning of the crystallization interval when the liquid was closer in composition to the bulk chondrule. For chondrules 20 and 111, zoning is limited in clinoenstatite, as discussed above, and the grain edges are in contact with mesostasis. Therefore, using the mesostasis composition to determine D* is not likely to introduce a large error. In chondrules 70 and 71, clinoenstatite is generally isolated from the mesostasis by orthopyroxene overgrowths and the bulk chondrule composition may be a more appropriate liquid to use for calculating D*. We have chosen to use mesostasis compositions for these minerals for consistency, as well as the fact that bulk chondrule compositions are variable, and we do not have good bulk chondrule compositional data for these specific chondrules. Within this constraint, we recognize that the D* values given for incompatible elements are likely to be minimum values because they probably crystallized from melts with lower incompatible element concentrations. Bulk chondrule REE concentrations are generally about 1–3 $\times$ CI (Grossman and Wasson 1983), so the values of D* given for clinoenstatite in these chondrules may be low by up to a factor of 10 for clinoenstatite.

Apparent partition coefficients for augite, orthopyroxene, and clinoenstatite are plotted in Figure 3 as a func-

TABLE 2. Compositions of chondrule pyroxenes: individual points

	Chondrule 20		Chondrule 70			Chondrule 111
	Cen*	Cen**	Aug†	Pig	Opx†	Aug
SiO_2	58.8	59.3	51.3	52.2	56.1	53.6
TiO_2	0.06	0.07	–	0.10	–	0.31
Al_2O_3	0.38	0.41	0.92	0.46	0.30	1.10
Cr_2O_3	0.58	0.66	1.81	1.61	0.72	2.66
FeO	1.63	1.81	18.1	21.0	13.7	6.34
MnO	0.23	0.27	1.16	1.31	0.58	0.87
MgO	38.5	37.92	10.8	18.6	28.5	17.5
CaO	0.20	0.25	14.9	3.52	0.35	16.6
Na_2O			–	0.13	–	0.64
Total	100.38	100.69	98.99	98.93	100.25	99.62

Notes: Aug = augite, Pig = pigeonite, Cen = clinoenstatite, Opx = Orthopyroxene. Blank spaces indicate concentration below detection limit.

* Analysis adjacent to SIMS spot, in core of clinoenstatite grain.

** Analysis adjacent to SIMS spot, at edge of same grain as 1.

† TiO_2 and Na_2O were not measured for these points.

TABLE 1—*Extended*

Chondrule 71		Chondrule 111		
Opx	Meso	Aug	Cen	Meso
56.2(0.5)	60.3(0.6)	52.4(0.6)	56.4(0.6)	65.8(1.5)
0.05(0.02)	0.45(0.01)	0.33(0.03)	0.02(0.01)	0.37(0.06)
0.40(0.17)	17.8(1.1)	1.2(0.1)	0.14(0.05)	10.1(0.9)
0.86(0.10)		2.1(0.1)	0.74(0.07)	0.26(0.25)
12.3(0.6)	8.4(1.4)	6.9(0.2)	7.1(0.7)	8.2(1.3)
0.50(0.04)	0.26(0.04)	0.89(0.04)	0.48(0.08)	0.60(0.06)
29.1(0.6)	0.17(0.15)	17.9(1.0)	32.8(0.7)	3.5(2.1)
0.56(0.17)	5.1(0.3)	16.4(0.9)	0.26(0.08)	4.7(2.0)
	6.4(0.29)	0.59(0.07)		4.4(1.1)
	0.31(0.09)			0.70(0.09)
0.017(0.001)	13.3(0.0)	2.38(0.12)	0.046(0.006)	7.03(0.41)
0.21(0.008)	9.9(0.8)	4.31(0.30)	0.065(0.010)	8.12(0.36)
0.031(0.004)	12.9(0.5)	2.82(0.17)	0.048(0.006)	7.52(0.16)
0.009(0.006)	12.5(1.7)	1.90(0.49)	0.007(0.003)	9.91(0.61)
0.015(0.007)	12.5(1.8)	1.95(0.14)	0.010(0.003)	9.14(0.35)
0.035(0.01)	12.8(1.8)	3.06(0.15)	0.016(0.013)	9.36(0.59)
0.045(0.03)	12.7(2.7)	3.96(0.63)		10.4(0.1)
	13.7(3.0)	3.26(0.55)		11.0(0.6)
0.093	11.6	4.49		9.22
0.191(0.48)	10.9(0.4)	5.10(1.48)		9.14(0.01)
0.226(0.31)	10.1(1.1)	5.11(1.69)		8.39(0.31)
0.248(0.15)	10.2(0.5)	3.56(0.50)		8.89(0.68)
79.9		53.4	88.7	
19.0		11.6	10.8	
1.1		35.1	0.5	
9, 1	6, 2	4, 1	9, 1	5, 2

tion of decreasing ionic radius for ions of ionic charge 2+, 3+, and 4+. For all valences, combined electron microprobe data and SIMS data show trends on these plots consistent with previous experimental and petrologic studies in similar systems (Kennedy et al. 1993; Yurimoto and Sueno 1987), giving confidence in the SIMS data.

Cr is strongly compatible in all pyroxenes, with values of D^* as high as 36 in augite in chondrule 70. No Cr data are plotted in Figure 3, because D^*(Cr) lies at least one, and often two or more, orders of magnitude above D^*(Al). All other minor elements measured are incompatible, except that Fe, Mn, and Ca are compatible in augite and D^*(Fe) and D^*(Mn) are approximately one in Ca-poor pyroxene. Also, values of D^* for Ti, Y, and Zr in augite all approach values of one and are thus potentially compatible. Values of D^* for REE vary from being extremely low, around 0.001 for LREE in Ca-poor pyroxenes, to close to one for HREE in augite, particularly in chondrule 20. Apparent partition coefficients for most trace elements increase with Wo content of pyroxene: values for pigeonite are intermediate between Ca-poor pyroxenes and augites.

Our data may be compared with those of Alexander (1994) for similar chondrules. In general, there is very close agreement between the data reported in this study and pyroxene-glass partition coefficients calculated from the data of Alexander (1994), for all elements and in all pyroxene minerals (Figs. 4 and 5). However, there are some important differences that are discussed in more detail below.

DISCUSSION

Apparent partition coefficients

Partition coefficients are known to be a complex function of melt composition, mineral composition, and temperature (Jones 1995). In particular, for pyroxenes, trace element partition coefficients are strongly dependent on the amount of Ca present in the mineral (Nielsen et al. 1992; McKay et al. 1986). In comparing our results with experimental data from the literature, it is important to take this effect into account and to use experimental studies which describe pyroxenes of appropriate Wo content. Green (1994) summarizes experimental trace element partition coefficient data. For Ca-poor pyroxene, a large range of partition coefficients is available from a variety

TABLE 3. Apparent partition coefficients (D*) for pyroxenes

	Chondrule 20		Chondrule 70				Chondrule 71	Chondrule 111	
	Aug	Cen	Aug	Pig	Opx	Cen	Opx	Aug	Cen
Ti	1.9(0.7)	0.15(0.05)	0.43(0.13)	0.20(0.04)	0.068(0.013)	0.045(0.009)	0.11(0.00)	0.89(0.15)	0.054(0.010)
Al	0.37(0.07)	0.023(0.000)	0.10(0.01)	0.07(0.01)	0.018(0.002)	0.008(0.001)	0.022(0.002)	0.12(0.01)	0.014(0.001)
Cr	12.3(3.6)	3.1(1.3)	36(129)	20(20)	14.6(14.9)	10.8(9.3)	>29	8.1(7.9)	2.8(2.8)
Fe	0.83(0.20)	0.78(0.18)	1.32(0.19)	1.32(0.18)	0.94(0.13)	0.79(0.11)	1.46(0.25)	0.84(0.13)	0.87(0.15)
Mn	1.1(0.2)	0.34(0.05)	1.9(0.5)	1.6(0.4)	0.98(0.27)	0.69(0.19)	1.9(0.3)	1.5(0.15)	0.80(0.10)
Ca	1.9(0.1)	0.025(0.01)	2.9(1.0)	1.0(0.4)	0.073(0.024)	0.028(0.009)	0.11(0.01)	3.5(1.5)	0.055(0.024)
Na	0.035(0.007)	—	0.073(0.012)	0.016(0.003)	—	—	—	0.13(0.03)	—
Sr	0.32(0.07)	0.002(0.000)	0.224(0.003)	0.020(0.000)	0.001(0.000)	0.005(0.000)	0.001(0.000)	0.338(0.020)	0.006(0.000)
Y	1.01(0.22)	0.005(0.001)	0.369(0.023)	0.074(0.004)	0.008(0.000)	0.004(0.000)	0.021(0.002)	0.531(0.025)	0.008(0.000)
Zr	0.83(0.16)	0.004(0.000)	0.186(0.007)	0.013(0.001)	0.002(0.000)	0.003(0.000)	0.002(0.000)	0.375(0.009)	0.006(0.000)
La	0.334(0.08)	0.001(0.000)	0.085(0.004)	0.006(0.000)	0.001(0.000)	0.002(0.000)	0.001(0.000)	0.191(0.014)	0.001(0.000)
Ce	0.406(0.106)	0.001(0.000)	0.149(0.003)	0.009(0.000)	0.001(0.000)	0.001(0.000)	0.001(0.000)	0.213(0.008)	0.001(0.000)
Nd	0.548(0.126)	0.001(0.000)	0.190(0.014)	0.009(0.001)	0.003(0.000)		0.003(0.000)	0.327(0.021)	0.002(0.000)
Sm	0.601(0.275)		0.252(0.021)				0.004(0.001)	0.380(0.007)	
Eu	0.493(0.171)		0.277(0.046)					0.297(0.019)	
Gd	0.869		0.293				0.008(0.000)	0.487(0.000)	
Dy	0.931(0.241)		0.340(0.032)	0.033(0.003)	0.011(0.001)	0.004(0.000)	0.018(0.003)	0.558(0.027)	
Er	1.035(0.339)	0.004(0.001)	0.341(0.032)	0.065(0.003)	0.012(0.001)		0.022(0.003)	0.609(0.063)	
Yb	0.790(0.212)	0.012(0.003)	0.302(0.008)	0.065(0.001)	0.013(0.000)	0.012(0.000)	0.024(0.001)	0.400(0.034)	

Notes: Aug = augite, Pig = pigeonite, Cen = clinoenstatite, Opx = orthopyroxene, Meso = mesostasis. Apparent partition coefficients are calculated as (mean composition of pyroxene)/(mean composition of mesostasis). Analytical precision errors are propagated from Table 1.

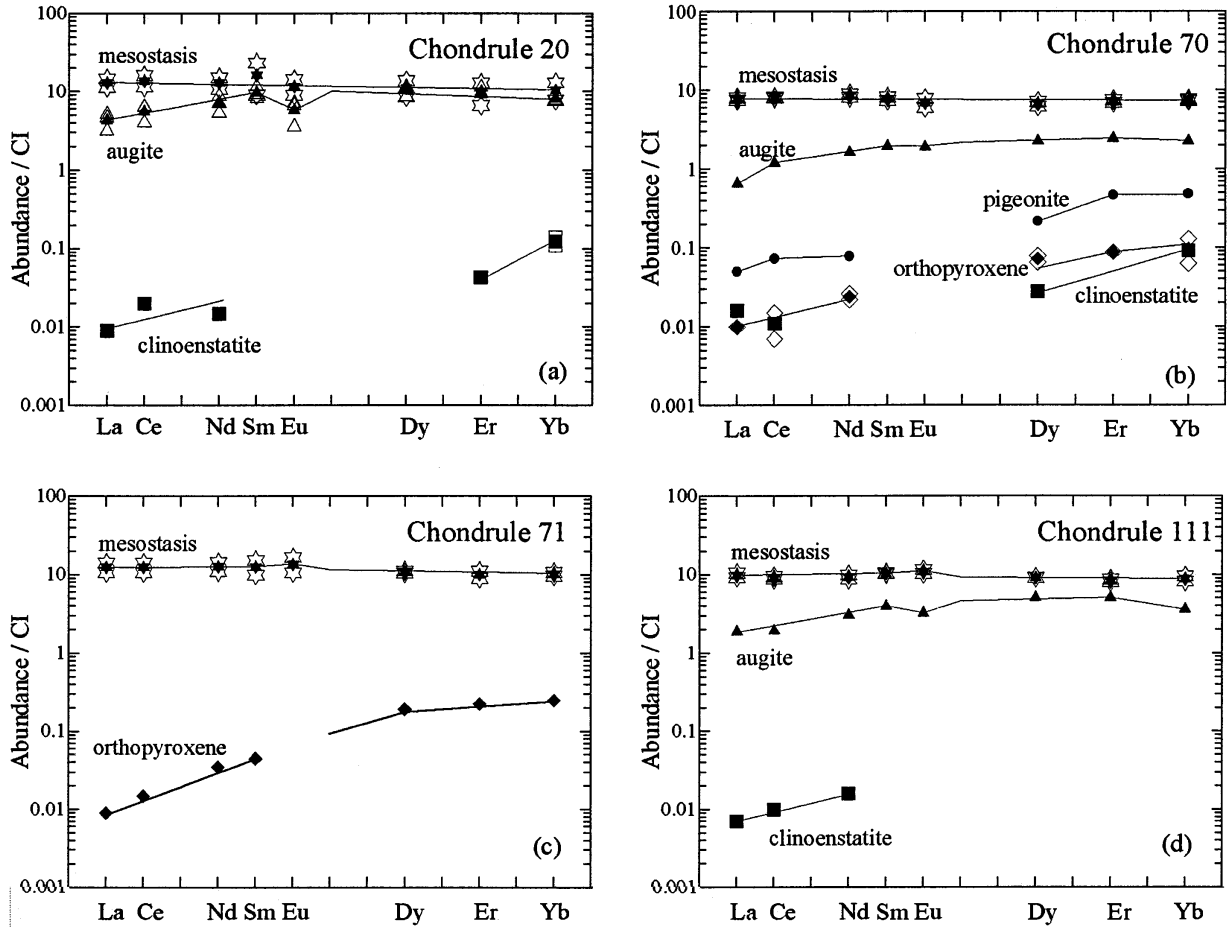

FIGURE 2. Abundances of REE in pyroxenes and mesostases in the four chondrules studied, relative to CI abundances (Anders and Grevesse 1989). Open symbols represent individual SIMS analyses and closed symbols are means for each pyroxene mineral. Elements that were below detection limits are not plotted. REE abundances in pyroxenes increase with increasing Wo content, and augites in chondrules 20 and 111 have small negative Eu anomalies. Mesostases are enriched in REE, to approximately 10 × CI abundances.

of studies. Data obtained by Kennedy et al. (1993) in chondrule analogue systems are generally very low. In comparison, several other experimental studies, the most comprehensive being that of Nielsen et al. (1992), determined partition coefficients up to two orders of magnitude higher for LREE and one order of magnitude higher for HREE. We interpret this large range as being due primarily to the Wo content of the pyroxenes studied: orthopyroxene in the Kennedy et al. study generally contains less than 0.2 mol% Wo, whereas orthopyroxene in the study by Nielsen et al. (1992) contains at least 2 mol% Wo. Data of Colson et al. (1988) span a range of partition coefficients, with the lowest Ca contents (<0.5 mol% Wo) being in close agreement with the data of Kennedy et al. (1993), and the highest Ca contents (up to 1 mol% Wo) similar to the data of Nielsen et al. (1992). Because our Ca-poor pyroxenes, both clinoenstatite and orthopyroxene, contain <0.5 and 0.5–1.0 mol% Wo respectively, we have chosen to compare our data with that of Kennedy et al. (1993), particularly as this study also used bulk compositions that were chondrule analogues.

Green (1994) shows that the range of experimentally determined partition coefficients for augites in a variety of bulk compositions is generally more limited than that for Ca-poor pyroxenes. The experimental data of Hart and Dunn (1993) for augites of composition around 45 mol% Wo generally lie in the middle of this range. McKay et al. (1986) also showed how partition coefficients in augite and pigeonite vary as a strong function of Wo content. We use these two sets of data for comparison with our chondrule data.

Values of D^* plotted in Figure 3 generally show smooth trends as a function of decreasing ionic radius, for ions of different valence states. On such a plot, the maximum in the curve matches the size of lattice sites in the mineral for cations of that ionic charge (Onuma et al. 1968). Experimental equilibrium data of Kennedy et al. (1993) for orthopyroxene in chondrule analog systems

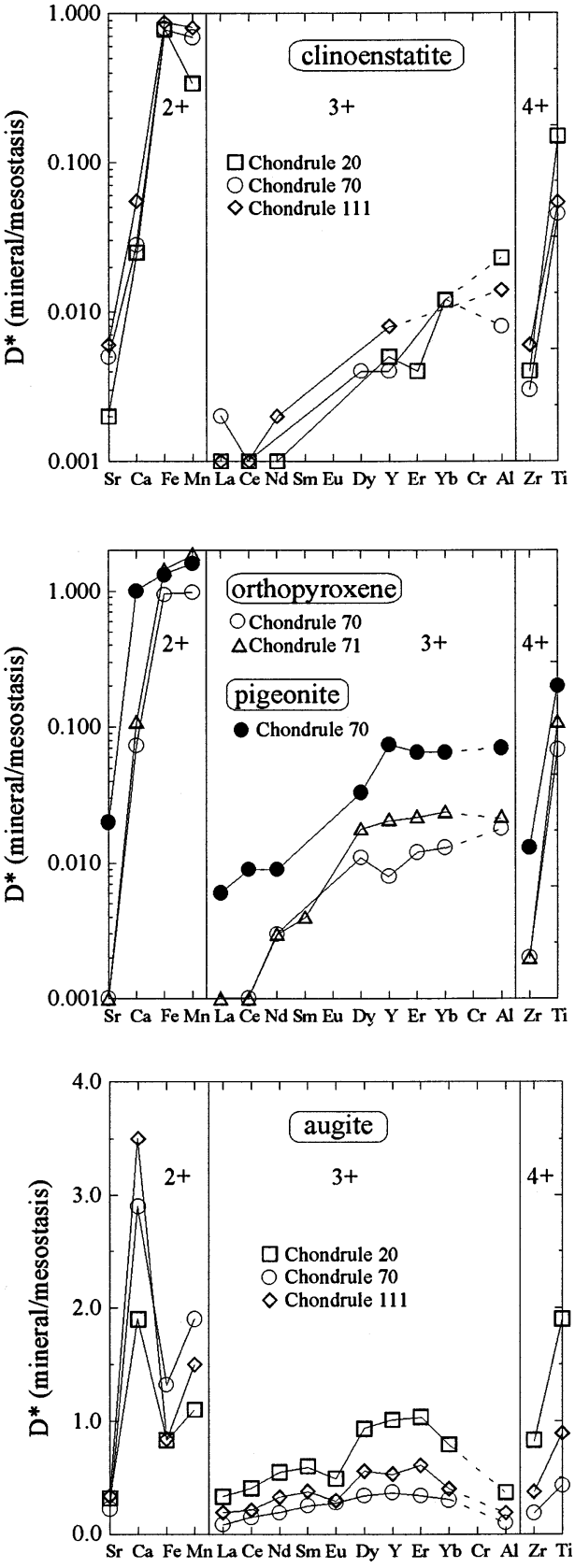

FIGURE 3. Apparent partition coefficients for clinoenstatite, orthopyroxene, pigeonite and augite plotted as a function of decreasing ionic radius for divalent, trivalent, and tetravalent cations.

→

show comparable trends to the clinoenstatite and orthopyroxene data in Figure 3. For divalent and tetravalent cations, increases in D^* in the order Sr → Ca → Fe ~ Mn and Zr → Ti are analogous to the Kennedy et al. trends. For trivalent cations, the observed smooth increases in D^* for REE with decreasing ionic radius, and values of D^*(Y) and D^*(Al) comparable to those of the heavy REE, are also consistent with equilibrium data. The maxima for divalent and trivalent cations in the Kennedy et al. (1993) data for orthopyroxene lie between Fe and Mn, and Yb and Al, respectively. We did not analyze elements with ionic radii intermediate between these points, but our data are consistent with these observations.

For augite, the pattern for divalent cations in Figure 3 differs from those of Ca-poor pyroxenes, in that D^*(Ca) is significantly higher than D^*(Fe) and D^*(Mn). This is consistent with data obtained by Yurimoto and Sueno (1987) for augite in a boninite, in which the maximum for divalent cations lies between Ca and Mn. The trivalent cations display a smooth pattern with a maximum around Y and Er. Deviations from this pattern for Eu are probably because Eu is present predominantly as a divalent, rather than a trivalent, cation. The ionic radius of Eu^{2+} is very similar to that of Sr^{2+}, so values of D^*(Eu) in augite are consistent with the divalent cation trend.

Chondrule cooling rates

Cooling rates of chondrules have been estimated by several methods, including the comparison of textures with those produced in dynamic crystallization experiments (Lofgren 1996; Hewins and Connolly 1996), comparison of olivine zoning properties with grains produced in experimental charges (Jones and Lofgren 1993; Yu et al. 1996), and the presence of high proportions of clinoenstatite as inversion products of the high-temperature polymorph, protoenstatite (Smyth 1974). For the porphyritic chondrules described here, cooling rates on the order of hundreds of degrees per hour are indicated (Jones 1994, 1996). These rapid cooling rates are clearly responsible for zoning in the phenocrysts, as well as the fact that the chondrules are highly disequilibrium assemblages. Below we investigate the possibility that rapid cooling may result in apparent partition coefficients that show significant departures from equilibrium.

Effect of cooling rate on apparent partition coefficients

The effect of rapid cooling on apparent partition coefficients has been recognized for some time (Albarede and Bottinga 1972), although the magnitude of expected effects is not well characterized. Because it is clear that

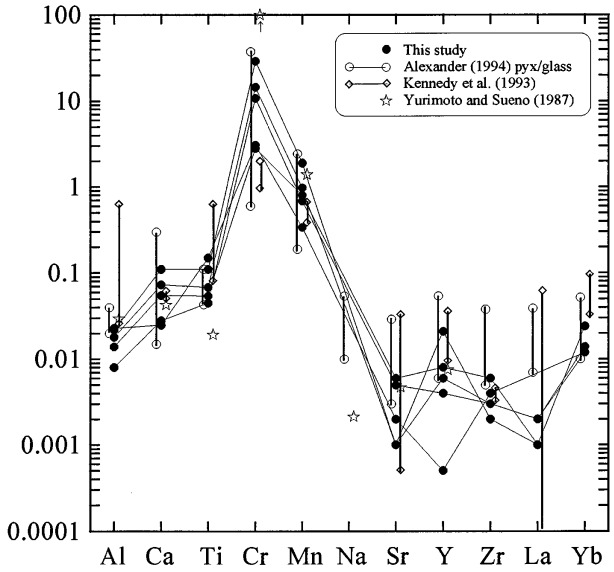

FIGURE 4. Apparent partition coefficients for Ca-poor pyroxenes (clinoenstatite and orthopyroxene), and a comparison with selected literature data for natural samples (Alexander 1994; Yurimoto and Sueno 1987) and synthetic material (Kennedy et al. 1993). Solid circles are pyroxene-mesostasis values from this study. Open circles show the ranges of values from Alexander (1994), calculated as pyroxene-glass from his data. The range for the Kennedy et al. data (open diamonds) represents an equilibrium experiment (RPII45: 2 K/h) and a rapidly cooled experiment (RP36: 2000 K/h); apparent partition coefficients for the equilibrium experiment are lower for all elements except Ca. Data from our study are generally in close agreement with the pyroxene-glass data calculated from Alexander (1994). For Al, Ti, Sr, Y, and Yb, these data plot near the equilibrium values from Kennedy et al.

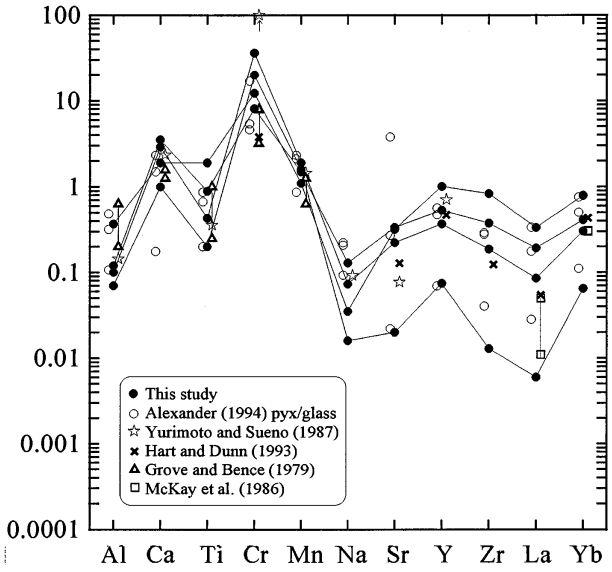

FIGURE 5. Apparent partition coefficients for Ca-rich pyroxenes, and a comparison with selected literature data for natural material (Alexander 1994; Yurimoto and Sueno 1987) and experimental studies (Hart and Dunn 1993; Grove and Bence 1979; McKay et al. 1986). Our data (solid circles) include three augites and one pigeonite, which has the lowest apparent partition coefficients for the incompatible elements. Open circles are individual analyses from Alexander (1994), calculated as pyroxene-glass. The lowest values of the Alexander data are for an analysis with intermediate Wo content which may be a pigeonite, or may be an overlapping analysis between enstatite and augite. The high value of D^* for Sr in one augite from Alexander is attributable to an anomalously low Sr content measured in glass for that chondrule. Data for La from McKay et al. (1988) are for Wo_{25} (lower value) and Wo_{45} (higher value).

the chondrules we have studied cooled rapidly, we can attempt to determine the effect of rapid cooling on partition coefficients by comparing our results with data from comparable equilibrium systems. Grove and Bence (1977, 1979) and Shimizu (1983) showed that partitioning of Al, Ti, and Cr between pyroxene (both Ca-poor pyroxene and augite) and liquid varies with cooling rate. The apparent partition coefficients of both incompatible (Al, Ti) and compatible (Cr) elements increase in rapidly cooled systems by factors of up to three. The effect of cooling rate on Ca-poor pyroxene partition coefficients for many trace elements in chondrule analogue systems was also investigated experimentally by Kennedy et al. (1993). This study showed that high cooling rates increase the apparent partition coefficients for many elements. However, for the orthopyroxene in their experiments, melt inclusions at a concentration of about 5% in crystals grown at rapid cooling rates may have compromised the trace element analyses, and a clear relationship between cooling rate and apparent partition coefficients was not established.

The ranges of mineral-glass partition coefficients for Ca-poor pyroxene determined by Kennedy et al. (1993) are shown in Figure 4 for an equilibrium experiment (carried out at a cooling rate of 2 K/h) and for one carried out at a cooling rate of 2000 K/h. In comparison with these experimental data, our apparent partition coefficients for Al and Ti in Ca-poor pyroxene are consistent with low cooling rates, and an approach to equilibrium (Fig. 4). Values of D^* for Sr and Yb data reinforce this interpretation. However, our data for Cr, as well as the values determined by Alexander (1994), are considerably higher than any obtained by Kennedy et al. (1993), even at very high cooling rates. Apparent partition coefficients for Al, Ca, Mn, Sr, and Y compare well with those measured for clinoenstatite ($Wo_{0.6}$) in a boninite (Yurimoto and Sueno 1987), although D^* for Ti is significantly lower in the boninite, and D^* for Cr is significantly higher.

For Ca-poor pyroxene, values of D^* for LREE, such as La, are considerably higher than the equilibrium data of Kennedy et al. (1993), and REE patterns for our data are considerably flatter (Figs. 4 and 6). It is possible that this pattern results from incorporation of 0.1% melt inclusions in a pyroxene with apparent partition coefficients similar to those measured in the equilibrium experiment by Kennedy et al. (1993). However, slopes of LREE pat-

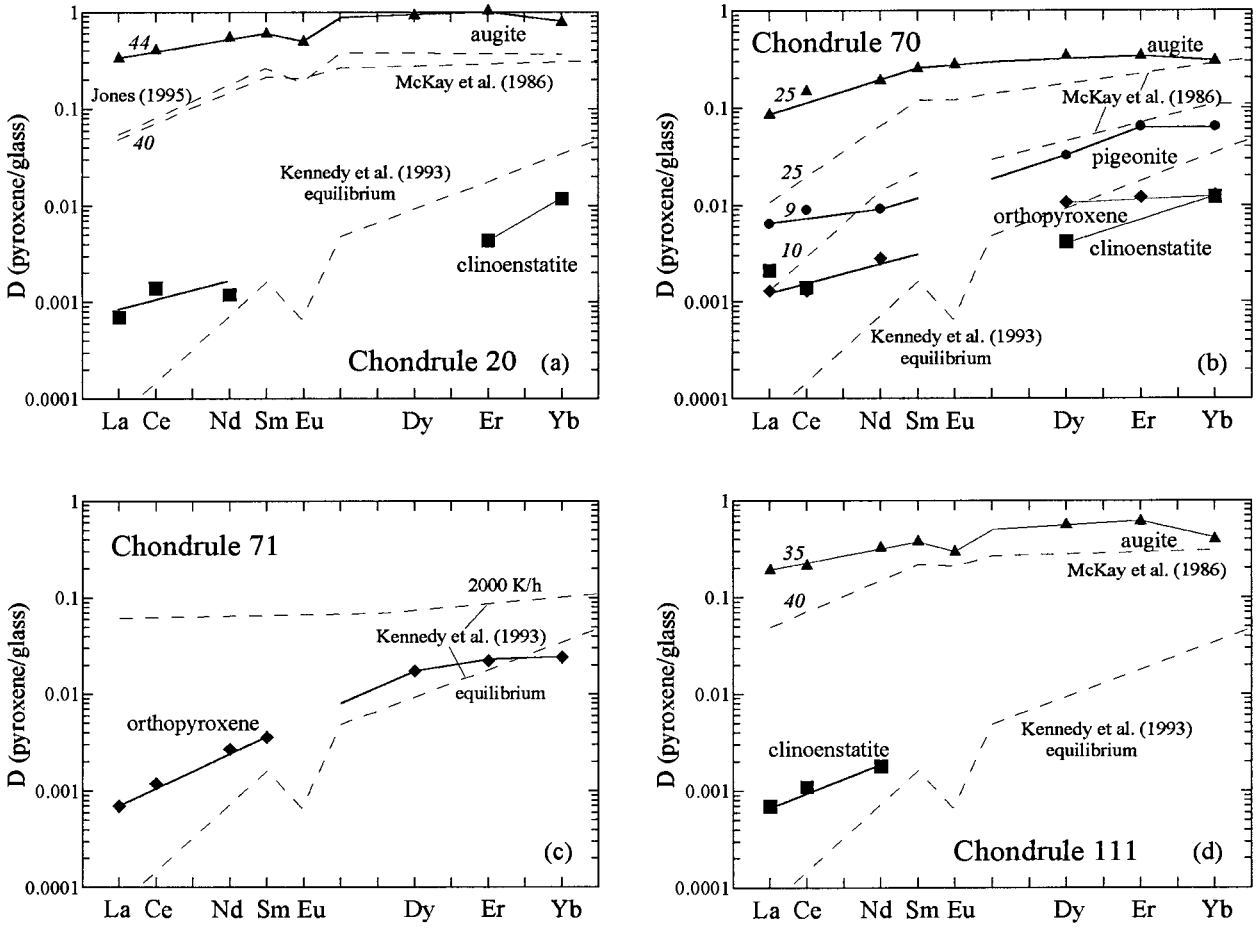

FIGURE 6. Apparent partition coefficients for REE in pyroxenes in the four chondrules studied, and comparisons with partition coefficients from Kennedy et al. (1993) for Ca-poor pyroxene, and McKay et al. (1986) and Jones (1995) for Ca-rich pyroxene. Data from McKay et al. (1986) are equilibrium data for varying Wo contents, which are labeled on the patterns. Partition coefficients for REE increase with Wo content of pyroxene. For all pyroxenes, slopes of the LREE patterns are similar and considerably flatter than equilibrium data. This may be attributable to the rapid cooling rates that chondrules experienced.

terns in Figure 6 are similar for all the pyroxene minerals studied in all four chondrules, suggesting that a similar process affected all pyroxenes and that the possibility that our analyses overlap small melt inclusions in Ca-poor pyroxenes is not a serious problem. The ratio of HREE/LREE values of D^* for Ca-poor pyroxenes was found to be even lower than our data by Alexander (1994), as illustrated in Figure 4. The differences between our data and those of Alexander (1994) for LREE are significant, approximately an order of magnitude. We do not have a good explanation for this because we apparently analyzed very similar objects in the same meteorite. Since our data clearly resolve Ca-poor pyroxenes, pigeonite, and augite in the same chondrules in a manner consistent with the respective Wo contents of these minerals, systematic analytical errors in our data appear to be unlikely.

Comparisons of our data for Ca-rich pyroxene with selected literature data from petrological and experimental studies are shown in Figs. 5 and 6. Values of D^* for all elements in chondrule augite, including LREE, are very similar to mineral-glass values calculated from the data of Alexander (1994). D^* for Al, Ti, and Mn are similar to those reported by Grove and Bence (1977, 1979) and Shimizu (1983), but D^* for Cr is higher than their values. For Al and Ti, the range of values we observe is greater than differences observed by Grove and Bence as a result of changes in cooling rate, so it is not possible to interpret the results in terms of cooling rates. Grove and Bence (1979) suggested that values of D^* for Ti close to one indicate that charge balanced substitutions are taking place between Ti and Al. Data for Al, Ca, Ti, Mn, Na, and Y are also very similar to data from boninites (Yurimoto and Sueno 1987), whereas, like Ca-poor pyroxenes, D^* for Cr in boninites is much higher than the values we measured. Differences in oxidation state between chondrules and boninites may account for large differences in the behavior of Cr: the higher f_{O_2} of boninites would be expected to result in a higher Cr^{3+}/Cr^{2+} ratio

than in chondrules, and partitioning of Cr^{3+} into pyroxene is favored relative to Cr^{2+} (Barnes 1986).

Values of D^* for Sr in augite are significantly higher than the data reported by Yurimoto and Sueno (1987) and experimentally determined values determined by Hart and Dunn (1993). However, our values are consistent with D^* for LREE, as expected from the normal geochemical behavior of Sr (Hart and Dunn 1993). Our value of D^* for La is also higher than values determined by Hart and Dunn, for relatively Ca-rich augite (Wo_{45}) and by McKay et al. (1986) for pyroxene with comparable Wo contents to ours (Wo_{25-40}; Figs. 5 and 6). However, our values of D^* for Y and Yb are comparable to both these studies. This lower ratio of Yb/La, or HREE/LREE, compared with equilibrium experimental data, is consistent with the relatively flat REE patterns in Ca-poor pyroxene discussed above. The relationship between Wo content and equilibrium partition coefficients defined by Jones (1995) gives values of D very similar to those determined by McKay et al. (1986; Fig. 6).

In summary, the HREE/LREE ratio appears to be markedly lower for all the pyroxenes we have measured in chondrules in comparison with experimental equilibrium data. The similarities in slopes of LREE patterns for all pyroxene minerals indicate that a common process has affected their REE partition coefficients: rapid cooling rates are suggested to be the most important factor producing this effect. The effect of rapid cooling on apparent partition coefficients for other elements is ambiguous from the data available.

Effect of composition

We suggest that our data may also show the effect of charge-balanced substitutions between Al and certain trace elements in augite, superimposed on the effect of cooling rate. As mentioned above, it has been suggested previously that values of D^*(Ti) close to one reflect charge balancing with Al (Grove and Bence 1979). For the chondrules in this study, values of D^* for all REE are significantly higher than equilibrium data, particularly in chondrule 20 in which values of D^* for augite are close to one for HREE (Fig. 6). This chondrule has notably high Al_2O_3 contents in both mesostasis and augite (Table 1), with 7 wt% Al_2O_3 in augite. Such high Al_2O_3 contents may increase the partitioning of trivalent REE ions because their uptake into the pyroxene crystal structure would be driven by charge balancing considerations (Colson et al. 1988, 1989; Gallahan and Nielsen 1992). Values of D* for Y in augite are similar to D^* for HREE as would be expected for an ion of the same charge and similar ionic radius (Fig. 3), and D^*(Y) is also higher in chondrule 20 than in the other two augites measured.

Acknowledgments

Constructive and helpful reviews by J. Beckett and H. Palme improved this manuscript considerably. We thank M. Spilde and G. Fowler for technical assistance. This work was supported by NASA Grant NAGW-3347 (J. Papike, P.I.) and the Institute of Meteoritics. Electron microprobe analyses were carried out at the Electron Microbeam Analysis Facility, Institute of Meteoritics and Department of Earth and Planetary Sciences, University of New Mexico. SIMS analyses were performed at the UNM/SNL Ion Microprobe Facility, a joint operation of the Institute of Meteoritics, University of New Mexico and Sandia National Laboratories.

References cited

Albarede, F. and Bottinga, Y. (1972) Kinetic disequilibrium in trace element partitioning between phenocrysts and host lava. Geochimica et Cosmochimica Acta, 36, 141–156.

Alexander, C.M.O'D. (1994) Trace element distributions within ordinary chondrite chondrules: Implications for chondrule formation conditions and precursors. Geochimica et Cosmochimica Acta, 58, 3451–3467.

———(1996) Recycling and volatile loss in chondrule formation. In R.H. Hewins et al., Eds., Chondrules and the Protoplanetary Disk, p. 233–241. Cambridge University Press, Cambridge, U.K.

Anders, E. and Grevesse, M. (1989) Abundances of the elements: Meteoritic and solar. Geochimica et Cosmochimica Acta, 53, 197–214.

Barnes, S.J. (1986) The distribution of chromium among orthopyroxene, spinel and silicate liquid at atmospheric pressure. Geochimica et Cosmochimica Acta, 50, 1889–1909.

Colson, R.O., McKay G.A., and Taylor, L.A. (1988) Temperature and composition dependencies of trace element partitioning: Olivine/melt and Ca-poor pyroxene/melt. Geochimica et Cosmochimica Acta, 52, 539–553.

———(1989) Charge balancing of trivalent trace elements in olivine and Ca-poor pyroxene: A test using experimental partitioning data. Geochimica et Cosmochimica Acta, 53, 643–648.

Gallahan, W.E. and Nielsen, R.L. (1992) The partitioning of Sc, Y and the rare earth elements between high-Ca pyroxene and natural mafic to intermediate lavas at 1 atmosphere. Geochimica et Cosmochimica Acta, 56, 2387–2404.

Green, T.H. (1994) Experimental studies of trace-element partitioning applicable to igneous petrogenesis—Sedona 16 years later. Chemical Geology, 117, 1–36.

Grossman, J.N. (1988) Formation of chondrules. In J.F. Kerridge and M.S. Matthews, Eds., Meteorites and the Early Solar System, p. 680–696. University of Arizona Press, Tucson, Arizona.

———(1996) The redistribution of sodium in Semarkona chondrules by secondary processes. Lunar and Planetary Science, XXVII, 467–468 (abstract).

Grossman, J.N. and Wasson, J.T. (1983) Refractory precursor components of Semarkona chondrules and the fractionation of refractory elements among chondrites. Geochimica et Cosmochimica Acta, 47, 759–771.

Grove, T.L. and Bence, A.E. (1977) Experimental study of pyroxene-liquid interaction in quartz-normative basalt 15597. Proceedings of the 8th Lunar Science Conference, 1549–1579.

———(1979) Crystallization kinetics in a multiply saturated basalt magma: An experimental study of Luna 24 ferrobasalt. Proceedings of the 10th Lunar Science Conference, 439–478.

Hart, S.R. and Dunn, T. (1993) Experimental cpx/melt partitioning of 24 trace elements. Contributions to Mineralogy and Petrology, 113, 1–8.

Hewins, R.H. and Connolly, H.C. Jr. (1996) Peak temperatures of flash-melted chondrules. In R.H. Hewins et al., Eds., Chondrules and the Protoplanetary Disk, p. 197–204. Cambridge University Press, Cambridge, U.K.

Irving, A.J. and Frey, F.A. (1984) Trace element abundances in megacrysts and the host basalts, constraints on partition coefficients and megacryst genesis. Geochimica et Cosmochimica Acta, 48, 1201–1221.

Jones, J.H. (1995) Experimental trace element partitioning. In T.J. Ahrens, Ed., Rock Physics and Phase Relations: A Handbook of Physical Constants, p. 73–104. American Geophysical Union.

Jones, R.H. (1994) Petrology of FeO-poor, porphyritic pyroxene chondrules in the Semarkona chondrite. Geochimica et Cosmochimica Acta, 58, 5325–5340.

———(1996) FeO-rich, porphyritic pyroxene chondrules in unequilibrated chondrites. Geochimica et Cosmochimica Acta, 60, 3115–3138.

Jones, R.H. and Lofgren G.E. (1993) A comparison of FeO-rich, porphyritic olivine chondrules in unequilibrated chondrites and experimental analogues. Meteoritics, 28, 213–221.

Kennedy, A.K., Lofgren, G.E., and Wasserburg, G.J. (1993) An experi-

mental study of trace element partitioning between olivine, orthopyroxene and melt in chondrules: equilibrium values and kinetic effects. Earth and Planetary Science Letters, 115, 177–195.

Lofgren, G.E. (1996) A dynamic crystallization model for chondrule melts. In R.H. Hewins et al., Eds., Chondrules and the Protoplanetary Disk, p. 187–196. Cambridge University Press, Cambridge, U.K.

Matsunami, S., Ninagawa, K., Nishimura, S., Kubono, N., Yamamoto, I., Kohata, M., Wada, T., Yamashita, Y., Lu, J., Sears, D.W.G., and Nishimura, H. (1993) Thermoluminescence and compositional zoning in the mesostasis of a Semarkona group A1 chondrule and new insights into the chondrule-forming process. Geochimica et Cosmochimica Acta, 57, 2101–2110.

McKay, G., Wagstaff, J., and Yang, S.-R. (1986) Clinopyroxene REE distribution coefficients for shergottites: The REE content of the Shergotty melt. Geochimica et Cosmochimica Acta, 50, 927–937.

Nielsen, R.L., Gallahan, W.E., and Newberger, F. (1992) Experimentally determined mineral-melt partition coefficients for Sc, Y and REE for olivine, orthopyroxene, pigeonite, magnetite and ilmenite. Contributions to Mineralogy and Petrology, 110, 488–499.

Onuma, N., Higuchi, H., Wakita H., and Nagasawa, H. (1968) Trace element partitioning between two pyroxenes and the host lava. Earth and Planetary Science Letters, 5, 47–51.

Sears, D.W.G., Huang, S., and Benoit, P. (1996) Open-system behavior during chondrule formation. In R. H. Hewins et al., Eds., Chondrules and the Protoplanetary Disk, p. 221–231. Cambridge University Press, Cambridge, U.K.

Shimizu, N. (1983) Interface kinetics and trace element distribution between phenocrysts and magma. In S.S. Augustithis, Ed., The Significance of Trace Elements in Solving Petrogenetic Problems and Controversies, p. 175–195. Theophrastus Publications, Athens, Greece.

Smyth, J.R. (1974) Experimental study of the polymorphism of enstatite. American Mineralogist, 59, 345–352.

Yu, Y., Hewins, R. H., and Zanda B. (1996) Sodium and sulfur in chondrules: Heating time and cooling curves. In R.H. Hewins et al., Eds., Chondrules and the Protoplanetary Disk, p. 213–219. Cambridge University Press, Cambridge, U.K.

Yurimoto, H. and Sueno, S. (1987) Anion and cation partitioning between three pyroxenes, chrome spinel phenocrysts and the host boninite magma: an ion microprobe study. Geochemical Journal, 21, 85–104.

Manuscript received May 27, 1996
Manuscript accepted January 31, 1997